Journal of Alloys and Compounds, *188* (1992) 259–263
JALCOM 9047

Crack growth resistance from natural crack lengths in polycrystalline alumina

M. Drissi-Habti and M. Gomina
LERMAT, URA CNRS 1317, ISMRa, 6 Bd du Maréchal Juin, 14050 Caen Cedex (France)

Abstract

The dye penetrant technique was used to measure crack lengths in the volume of SENB specimens of polycrystalline alumina tested using three-point bending. The incremental work of fracture was calculated from these crack length values assuming linear elastic behaviour (G_R^*), and the R curve was derived taking into account linear non-elastic behaviour ($G_R^* = \phi + \tilde{G}$). In the first case the incremental work of fracture starts from 26 J m^{-2} and increases up to a plateau value of 73 J m^{-2}, while in the second case the resistance increases continuously. Crack mouth bridging by grains partially pulled out is shown to be at the origin of these R curves, the increase in which was used to evaluate the bridging stress in the wake of the propagating crack. The cumulated number of counts in acoustic emission ΣN is shown to be a linear function of the macroscopic crack extension Δa.

1. Introduction

It is now well known that the thermomechanical characteristics of structural ceramic materials such as the subcritical crack growth, cyclic fatigue and thermal shock resistance are strongly dependent on the R curves (increase in crack growth resistance with crack extension). Hence direct and reliable methods established for model materials are needed to calculate the R curve; these methods should then be applied to study reinforced ceramic-matrix materials. Crack propagation mechanisms in polycrystalline ceramics have been intensively studied, and it is recognized that damage proceeds by the formation of a frontal "process zone", the extension of which induces the R curve behaviour. Following on the work of Knehans and Steinbrech [1], who showed the effect of this frontal process zone on the R curve behaviour, Evans and Faber [2] evaluated the extent of microcracking effects in the frontal zone of a propagating crack on the R curve and concluded that other mechanisms may occur, depending on the nature and the microstructure of the material (microcracking induced dilatation, crack mouth bridging in the wake, etc.). For polycrystalline graphite, Sakai [3] showed that the contributions of the frontal process zone and the crack wake (microcrack and coarse grain bridging) to the fracture energy are more important than the elastic energy released by the creation of crack surfaces; electronic microscopy observations revealed an extended bridging zone behind the crack tip. Steinbrech *et al.* [4, 9] checked the effects of bridging on the R curve for coarse-grained alumina and observed that the rising R curve was correlated with the roughness of the crack surfaces. The crack tip energy was independent of the notch depth and crack length (21 J m^{-2}) whereas the plateau resistance level (100 J m^{-2}) reached after a crack extension of 2.5 mm was governed by the wake region.

In this paper we propose an R curve and work of fracture measurements for polycrystalline alumina based on experimental measured crack lengths inside the specimens, using the linear elastic method and a linear non-elastic model.

2. Materials and experimental details

2.1. Material and metallographic preparation

The material used was a high purity polycrystalline alumina (99.7%) with mean grain size of 20 μm. Some physical characteristics given by the manufacturer are listed in Table 1.

TABLE 1. Physical characteristics of the Al_2O_3 material, given by the manufacturer

Ultimate flexural stress σ (MPa)	250 220 at 800 °C
Elastic modulus E (GPa)	310
Toughness K_{IC} (MPa m$^{1/2}$)	4.6
Weibull modulus m	25
Poisson's ratio ν	0.27
Linear expansion coefficient α ($\times 10^5$ °C^{-1})	
Ultimate compression stress (MPa)	800 1500 at 800 °C

0925-8388/92/$5.00

The specimens were polished using a diamond paste of different grain size (8, 6, 3 and 1 μm) to allow microscopy observation of the crack path. SENB specimens of dimensions $L = 77$ mm, $W = 8$ mm, $B = 4$ mm were tested using three-point bending with a span to depth ratio $L/W = 8$. The notch was machined using a copper saw of thickness 100 μm, the relative notch depth was $a_0/W = 0.4$ for all the specimens.

2.2. Experimental procedure

The mechanical tests were displacement controlled ($V_T = 10$ μm min^{-1}) and run using a Schenck RMC type testing machine with a load cell capacity of 10 kN. Preliminary tests using four-point bending did not allow stable crack propagation to be obtained. A Dunegan 3000 series acoustic emission set with a piezoelectric transducer with a bandwidth of 1 kHz–1 MHz was used, the threshold level was 30 dB and the gain 50 dB. The crack path on the surface of the specimen was monitored using an optical microscope, the sharpest observations and analysis of the surfaces of rupture were conducted using a Jeol 840 scanning microscope. The crack front was revealed in the volume of the specimen using a coloured dye.

The usual derivation of an R curve from a controlled crack propagation load–displacement plot is based on two main assumptions: (i) the material behaves as totally linear elastic; (ii) for a given compliance value, the instantaneous crack length is assumed to be identical with the crack length estimated from the calibration curve obtained from saw-cut notches. However, the presence of contacts between grains behind the crack tip (the crack mouths are not stress free) invalidates this equivalence. First, we measured the natural crack lengths all along the loading curves, and used these to calculate the incremental work of fracture G_R^* assuming linear elastic behaviour. The crack growth resistance G_R was also calculated assuming linear non-elastic behaviour.

2.2.1. Crack length measurement

Identical specimens with $a_0/W = 0.4$ were monotonically loaded to different preset load values P_i. After unloading the specimen was reloaded until the reloading loop met the previous unloading loop. The usual linear elastic compliance value C_i^* is obtained by joining the origin to the unloading point. The local compliance C_i is then estimated using the tangent line to the reloading loop through the unloading point (Fig. 1). The optical crack length Δa_{op} was measured on the surface of the loaded specimen using an optical microscope. The crack length in the volume of the specimen Δa_i was obtained a few days later from the mark of a penetrant dye poured into the notch root after the test. Thus, the specimen stressed under a load P_i has a crack extension Δa_i and a local compliance C_i. Figure 2 shows the envelope of the partial loading curves, with the crack growth increments Δa_i. These crack growth increments Δa_i are plotted in Fig. 3 as a function of the applied load values P_i. No crack growth was observed on the surface or in the volume of the specimens unless the maximum load value were reached. However, microcracks were observed around the notch root (up to

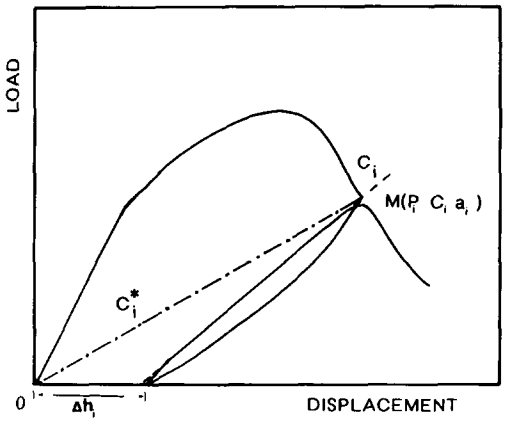

Fig. 1. Illustration of the compliances C_i^* and C_i.

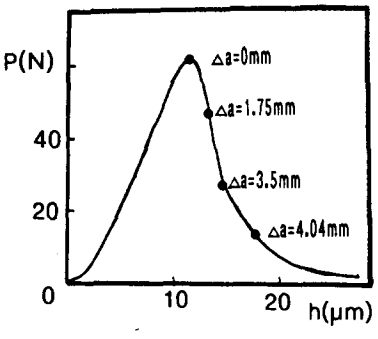

Fig. 2. Envelope of partial loading curves with crack growth increments Δa_i.

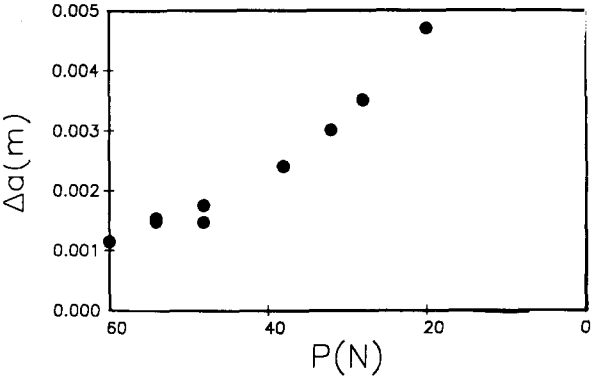

Fig. 3. Crack growth increment Δa_i plotted as a function of the applied load.

270 μm ahead) when the specimen was unloaded from a point in the non-linear region just before P_{max}.

2.2.2. Incremental work of fracture measurements

Monotonic loading curves are used to calculate the incremental work of fracture G_R^*:

$$G_R^*(a_i) = \frac{\int_{a_{i-1}}^{a_i} P \, dh}{B(a_i - a_{i-1})} \quad (1)$$

where the integral represents the mechanical energy needed to extend the crack from a_{i-1} to a_i. The integral over the total remaining ligament $(w - a_0)$ gives the usual work of fracture 2γ.

The residual displacements shown on loading–unloading curves (as depicted schematically in Fig. 4) are used to work out the fracture energy G_R assuming linear non-elastic behaviour. These irreversible displacements Δh originate from the frontal process zone and the crack wake as an effect of bridging of the crack by the grains. The local compliance value C is expressed as:

$$C = C^* - \frac{\Delta h}{P} \quad (2)$$

and the fracture energy is divided into two parts as proposed by Eftis *et al.* [5] and further applied by Sakai *et al.* [6]:

$$G_R = \tilde{G} + \phi \quad (3)$$

with

$$\tilde{G} = \frac{P^2}{2B}\left(\frac{\partial C}{\partial a}\right) \quad (4a)$$

and

$$\phi = \frac{P}{B}\left(\frac{\partial \Delta h}{\partial a}\right) \quad (4b)$$

$\tilde{G}$ is the rate of energy dissipated for the creation of new crack surfaces, whereas ϕ is the rate of energy consumed in non-elastic processes during crack extension (Fig. 4).

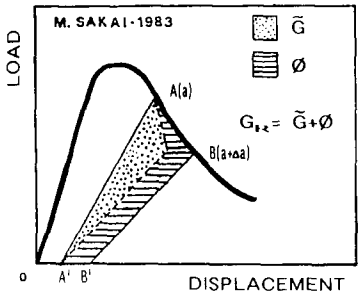

Fig. 4. Illustration of the superposition method.

3. Results and discussion

3.1. Incremental work of fracture and resistance curve

Figure 5 shows the G_R^* values as a function of the crack extension Δa. From a crack initiation value $G_0 = 26\ J\ m^{-2}$, the G_R^* curve rises to a plateau level of $73\ J\ m^{-2}$. In their pioneering paper revealing the R curve effect in polycrystalline alumina, Hübner and Jillek [7] predicted that the toughness should increase in some materials by a factor of up to 3 or 4 after a few millimeters of crack extension, as a consequence of the formation of a frontal microcrack zone and the development of the crack wake. The results presented in Fig. 5 confirm these assumptions. The plateau level of $73\ J\ m^{-2}$ is reached after a crack extension of 3 mm, slightly higher than the 2.5 mm reported by Steinbrech *et al.* [4] for a similar material tested using compact tension specimens. The difference between the crack growth initiation energy ($26\ J\ m^{-2}$) and the work of fracture ($73\ J\ m^{-2}$) is the result of subsequent microcracking ahead of the macrocrack and from its wake.

To obtain insight into the amount of energy dissipated in non-elastic processes, the incremental work of

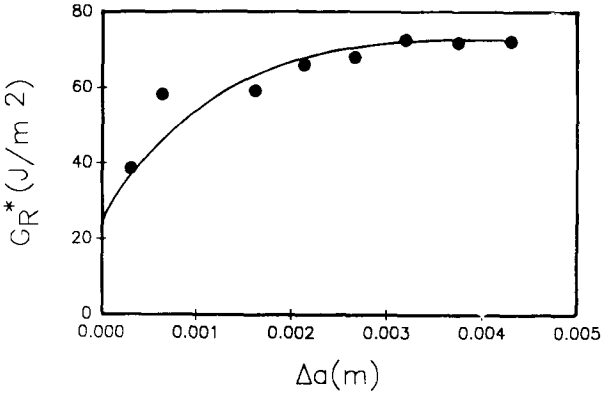

Fig. 5. G_R^* values plotted as a function of crack extension Δa_i.

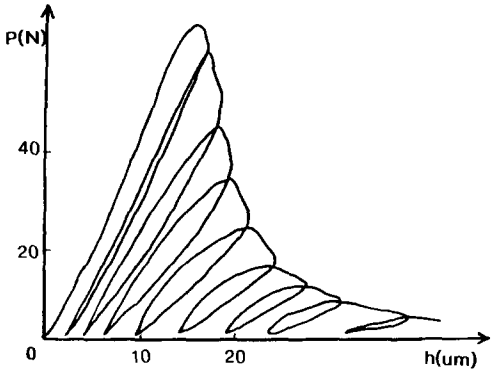

Fig. 6. An example of loading–unloading curves for Al_2O_3 material.

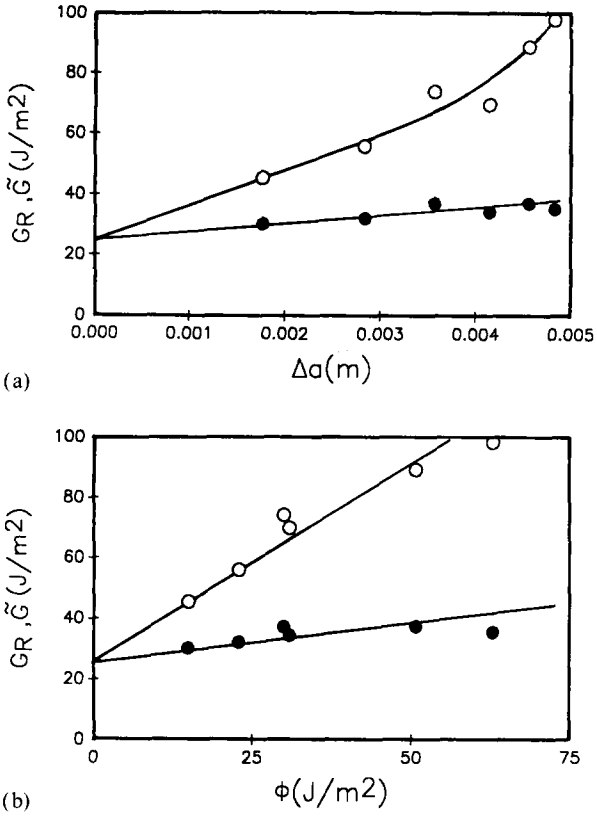

Fig. 7. G_R and $\tilde{G}$ as a function of (a) the crack growth increment Δa and (b) the non-elastic energy rate ϕ.

fracture G_R and the quasi-elastic energy $\tilde{G}$ gained from loading–unloading curves (Fig. 6) are plotted in Fig. 7(a) as a function of the crack growth increment Δa. It is clearly seen that the non-elastic term ϕ increases continuously as the crack grows; the ratio of the incremental work of rupture G_R over the quasi-elastic contribution $\tilde{G}$ varies from 1 to 2.7. Extrapolations by linear regression on the plots of G_R and $\tilde{G}$ values as a function of ϕ to $\phi = 0$ (Fig. 7(b)) exhibit an initiation energy $(G_R)_0 = (\tilde{G})_0 = G_0 = 26\ \mathrm{J\ m^{-2}}$, the same as that obtained in Fig. 5. In this study, the behaviour of the material was considered linear elastic or linear non-elastic, thus the hysteresis effects demonstrated by the presence of loading–unloading loops which are mainly due to microdisplacements and friction between the interlocking grains in the crack wake were neglected (Fig. 8). The energy dissipated associated with these mechanisms may be enhanced by subcritical crack growth under air, depending on the nature of the sintering additives.

Following new developments in the analysis of the crack bridging contribution to the toughness of ceramics, the bridging stress σ_b is evaluated from the experimentally measured R curve using the Irwin relation

$$G_R = \frac{K_R^2(1-\nu^2)}{E} \tag{5}$$

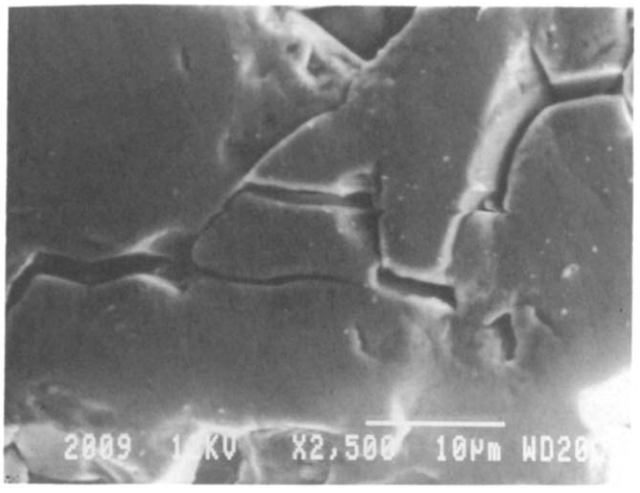

Fig. 8. Scanning electron micrograph showing an example of bridging of crack mouths by grains partially pulled out.

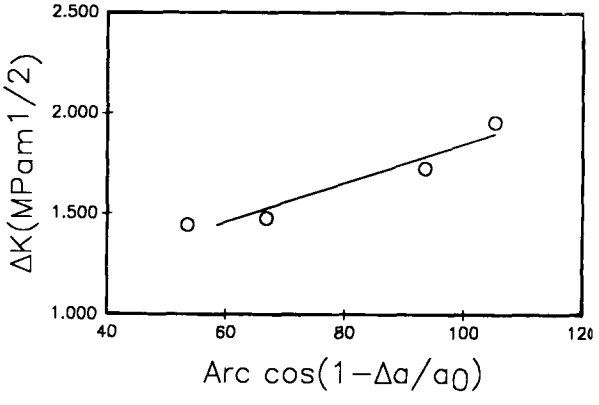

Fig. 9. ΔK plotted as a function of crack growth increment Δa.

and assuming that the increase in K_R curve is due only to bridging effects

$$K_R = K_{ini} + \Delta K \tag{6}$$

The increase ΔK is modelled using the modified Dugdale approach of uniform traction stress σ_b [8]:

$$\Delta K = \sigma_b\left(\frac{4\sigma_b}{\pi}\right)^{1/2} \arccos\left(1 - \frac{\Delta a}{a_0}\right) \tag{7}$$

Figure 9 illustrates relation (7) for the crack extension prior to the plateau level ($\Delta a \leqslant 3$ mm). From the slope of the best fitted line, we calculate $\sigma_b = 153$ MPa. This high value of the mean bridging stress suggests that other contributing mechanisms such as microcracking should be considered as well as the shielding of the crack tip by interlocking grains.

3.2. Acoustic emission

The correlation of the monotonic loading curves with the cumulated number of counts in acoustic emission (Fig. 10) shows 3 zones.

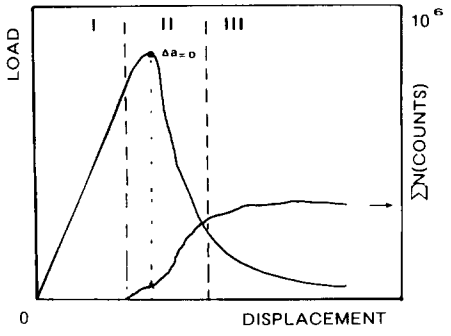

Fig. 10. Correlation of monotonic loading curve with the cumulated number of counts in acoustic emission.

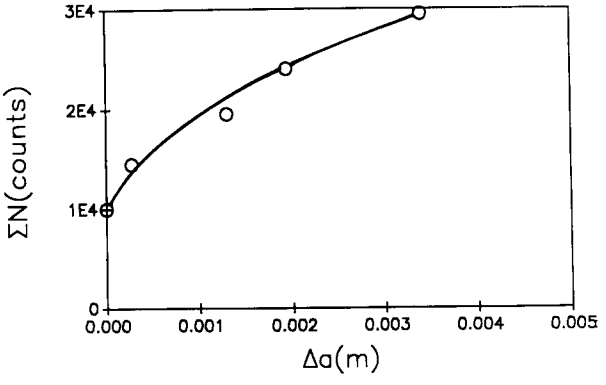

Fig. 11. The cumulated number of counts ΣN plotted as a function of crack growth increment Δa.

In zone I the specimen behaves as linear elastic, there is no acoustic signal.

Acoustic emission appears in zone II although the loading curve is still linear. The increase in the rate of acoustic emission before the maximum load value then corresponds to the formation of a damaged zone around the notch tip and not to the occurrence of subcritical crack growth since no crack growth is revealed before the maximum load value is reached ($\Delta a_{op} \equiv 0$, $\Delta a_i \equiv 0$, microcracked zone size approximately 270 μm). The further increase in the acoustic emission is due to the rapid propagation of the macroscopic crack created at P_{max}.

In zone III the total number of counts reaches saturation level, the specimen is completely fractured.

According to these observations, we plotted the cumulated number of counts ΣN as a function of the macroscopic crack length Δa (Fig. 11).

Since the dimensions of the specimens tested are large enough for valid measurements of fracture parameters, the $\Sigma N = f(\Delta a)$ relation shown in Fig. 11 should be particular to the given material. It can be used in combination with loading curves to estimate crack growth resistance curves for specimens of other dimensions made of the same material.

4. Conclusion

The crack growth resistance curve and the work of fracture were derived for polycrystalline alumina based on the crack length values measured in the volume of the specimens. A work of fracture of 73 J m^{-2} was reached after a crack extension $\Delta a = 3$ mm, while the crack growth initiated at $G_0 = 26$ J m^{-2}. The increase in the R curve is attributed to the interlocking grains in the crack wake, although the crack surface bridging stress is overestimated (153 MPa) when assuming a uniform value all along the crack length.

References

1 R. Knehans and R. Steinbrech, *J. Mater. Sci. Lett.*, *1* (8) (1982) 327–329.
2 A. G. Evans and K. T. Faber, *J. Am. Ceram. Soc.*, *67* (4) (1983) 255–260.
3 M. Sakai, *J. Am. Ceram. Soc.*, *71* (8) (1988) 609–616.
4 R. W. Steinbrech, A. Reichl and W. Schaarwächter, *J. Am. Ceram. Soc.*, *73* (7) (1990) 2009–2015.
5 J. Eftis, D. L. Jones and H. Liebowitz, *Eng. Fr. Mech.*, *7* (1975) 491–503.
6 M. Sakai, K. Urashima and M. Inagaki, *J. Am. Ceram. Soc.*, *66* (12) (1983) 868–874.
7 H. Hübner and W. Jillek, *J. Mater. Sci.*, *12* (1977) 117–125.
8 T. Miyajima and M. Sakai, *J. Mater. Res.*, *6* (3) (1991) 539–547.
9 R. W. Steinbrech, R. Knehans and W. Schaarwächter, *J. Mater. Sci.*, *18* (1983) 265–270.